An Embedded Voltage Harmonic Compensation Strategy for Current Controlled DG Interfacing Converters

Zhao, Xin; Meng, Lexuan; Guerrero, Josep M.; Savaghebi, Mehdi; Quintero, Juan Carlos Vasquez; Xie, Chuan; Wu, Xiaohua

Published in:
Proceedings of 8th Annual IEEE Energy Conversion Congress and Exposition (ECCE) 2016

DOI (link to publication from Publisher):
10.1109/ECCE.2016.7854841

Publication date:
2016

Document Version
Early version, also known as pre-print

An Embedded Voltage Harmonic Compensation Strategy for Current Controlled DG Interfacing Converters

Xin Zhao, Lexuan Meng, Josep M. Guerrero, Mehdi Savaghebi, Juan C. Vasquez
Department of Energy Technology
Aalborg University, Denmark
{xzh, lme, joz, mes, juq}@et.aau.dk

Chuan Xie
School of Automation Engineering,
University of Electronic Science and Technology of China
Chengdu, China
c.xie@uestc.edu.cn

Xiaohua Wu
School of Automation
Northwestern Polytechnical University
Xi'an, China
wxh@nwpu.edu.cn

***Abstract*—Harmonics have been considered as one of the major issues in future power grids. With the increasing demand in advanced control functions, power electronic converter interfaced Distributed Generators (DGs) are expected to perform harmonic compensation when necessary. It has been demonstrated in a number of studies that DG converters operating in Voltage-Controlled Mode (VCM) can be easily configured to realize voltage harmonic suppression utilizing naturally embedded voltage control loop. While for DG converters operating in Current-Controlled Mode (CCM), such function was rarely studied. Considering that CCM is commonly used in renewable energy based generators and energy storage systems, it has certain significance to achieve the same function with CCM operated converters. Aiming at such objective, this paper proposes a voltage detection based embedded Harmonic Compensator (HC) for CCM converters. The novelty and main advantages of the proposed method include: 1) it realizes seamless interface of HC with inner fundamental current control loop; 2) compared with conventional active power filtering method, it does not require remote load harmonic current measurement since it is based on local voltage detection; 3) compared with conventional voltage detection based method, it offers better performance because of direct harmonic voltage regulation. Experimental results are presented to demonstrate the effectiveness of the method.**

Keywords—distributed generator; current-controlled mode; active power filtering; voltage harmonic compensation.

I. INTRODUCTION

Current-controlled power converters are usually used for interfacing renewable energy sources (RES) and energy storage systems (ESS) into power grid. Apart from basic current/power control, advanced functions, such as reactive power compensation and active power filtering [1], can also be realized by properly programming those converters.

Focusing on harmonic compensation issues, a number of research works have been proposed. In [2], a load current detection based active power filtering strategy is proposed to compensate the harmonic load current. However, since the load in a real power grid is highly distributed, the load current can hardly be measured and thus the application of this scheme is relatively limited. To overcome this issue, a harmonic compensation strategy based on local voltage measurement is proposed in [3], but this scheme suffers from poor performance issues. A critical load bus voltage harmonic mitigation method is proposed using a hierarchal control scheme in [4]. Although the power quality at the selected bus can be improved, it can hardly be applied to DG converters since it requires the converters operating in Voltage-Controlled Mode (VCM). Similar approach can be also found in [5] with VCM based control.

Considering that Current-Controlled Mode (CCM) is commonly used in renewable energy based generators and energy storage systems, it has certain significance to achieve the same function with CCM based converters. The novelty of this paper is to realize voltage harmonic compensation by using CCM converters in either islanded or grid connected systems. The converter is programmed to act as a multi-functional device which has the capability of both regulating power generated from the RES and compensating voltage harmonics caused by non-linear loads. Compared with the conventional methods, the proposed approach can achieve high voltage harmonic compensation performance by only using locally measurable feedback signals.

The rest of the paper is organized as follows. Section II gives a brief introduction to the conventional harmonic mitigation strategies while Section III illustrates the proposed control scheme. Section IV provides the design and stability analysis of the proposed control scheme. Experimental results is analyzed and discussed in Section V. Finally, Section VI presents the conclusion of the paper.

II. CONVENTIONAL HARMONIC COMPENSATION STRATEGY

The common idea of Point of Common Coupling (PCC) voltage harmonic suppression is achieved by controlling the DG converters to generate harmonic current which has the same amplitude and phase angle with load harmonic current, therefore only the fundamental current flows into the grid resulting in a better PCC voltage. The conventional harmonic

This work was supported by the Danish Energy Technology Development and Demonstration Program (EUDP) through the Sino-Danish Project "Microgrid Technology Research and Demonstration", and by the International Science & Technology Cooperation Program of China, project Number: 2014DFG62610, and also by Fundamental Research Funds for the Central Universities, project number: ZYGX2014J069.

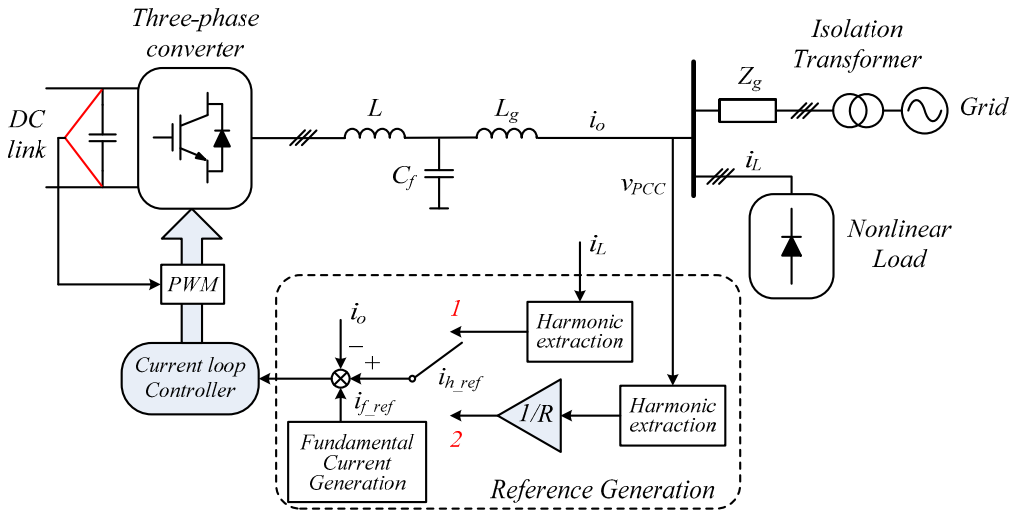

Fig. 1. Conventional harmonic compensation strategy.

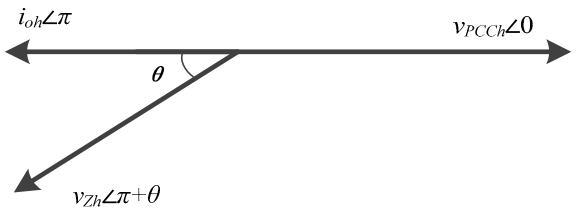

Fig. 2. Phasor diagram at harmonic frequencies of the DG system.

compensation strategy using a DG converter is shown in Fig. 1. The converter is shunt connected to the grid through a *LCL* filter, and Z_g stands for the grid impedance. Nonlinear loads are connected at PCC.

As can be seen from Fig. 1, the control block includes a current loop controller and a current reference generation block. In general, repetitive controller (RC) or proportional + resonant (PR) controller can be used as the current controller to provide high gains at harmonic order frequencies, achieving accurate tracking of harmonic current components. In harmonic current reference generation block, two different approaches are usually applied. The first approach measures the load current (i_L) and extracts the harmonic components for using as compensation references. In this case, the DG converter operates similarly with a shunt active power filter (APF). In the second approach, the DG converter is controlled to absorb a current proportional to the instantaneous PCC harmonic voltage. Thus, the DG converter can be regarded as a resistive APF which providing a low-impedance path for harmonic currents.

The second approach avoids remote load current measurement, since only local voltage information is needed. However, since the DG converter presents a resistive feature at harmonic frequencies, the injected harmonic current will not be in phase with the voltage drop across the grid impedance, as shown in Fig. 2, which degrades the effectiveness of the compensation performance. In this figure, θ denotes the angle of grid impedance, i_h represents the harmonic current injected by the DG converters, v_{PCCh} stand for the harmonic voltage at PCC while v_{Zh} denotes the voltage drop across the grid impedance. Otherwise, the phase angle of the injected harmonic current needs to be optimized based on the accurate measurement of grid impedance [6], which is considered not practical.

III. Proposed Harmonic Compensation Strategy

Due to the aforementioned drawbacks of the conventional harmonic compensation scheme, a novel control algorithm, which consists of a voltage Harmonic Compensator (HC) as well as a fundamental current controller, is proposed in this paper, and the corresponding control scheme is shown in Fig. 3. The studied system consists of a CCM converter connected to PCC through a *LCL* filter, a three phase diode rectifier based nonlinear load, and a voltage terminal which can be either a power grid or a VCM converter. Note that K is the harmonic voltage feedback gain. To achieve harmonic mitigation by only using locally measurable signals, the capacitor voltage is taken as the feedback control variable.

Single-line equivalent circuit of the studied system is illustrated in Fig. 4, where i_{oh} and i_{Lh} are the harmonic components of the converter output current and load current, respectively, Z_{oh} is the converter output impedance at h^{th} order harmonic, and v_{ch} is the harmonic voltage of filter capacitor. Assuming that the converter can track the harmonic voltage without steady-state error, the phasor diagram of the system can be shown in Fig. 5. Note that i_{PCCh} denotes the grid harmonic current, and the sign of m and n is determined by K. As illustrated in Fig. 5, if v_{ch} is counter phase with v_{PCCh}, the voltage difference between filter capacitor and PCC increases which results in the harmonic compensation operation of the converter. Otherwise, if v_{ch} is in phase with v_{PCCh}, the voltage difference between filter capacitor and PCC decreases, consequently, the converter will operate in harmonic rejection mode. It is worth noting that when v_{ch} equals to v_{PCCh} the harmonic current will only be provided by the grid. However, since the capacitor voltage cannot perfectly track its reference in real cases, part of the harmonic current will still flow into the converter. The influence of K on i_{oh} is illustrated by deriving the following equation:

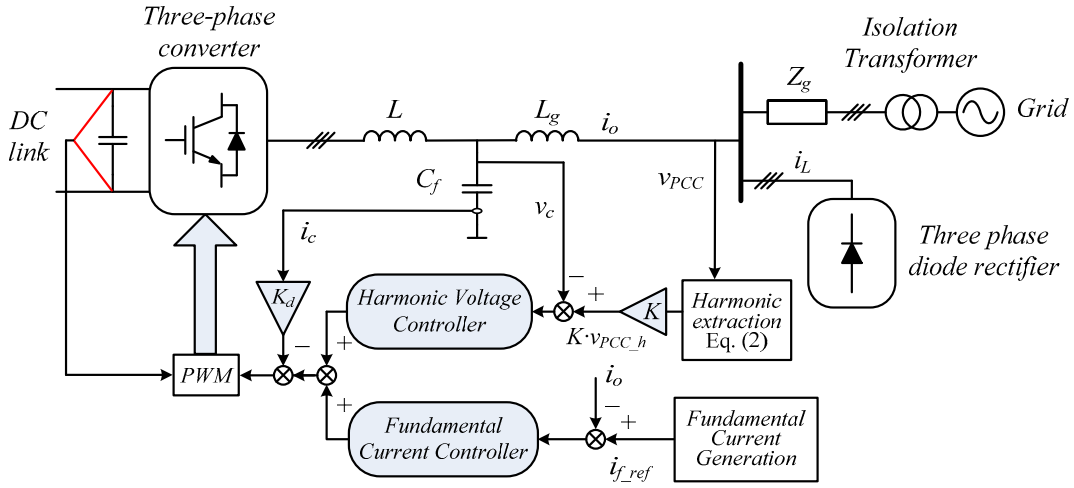

Fig. 3. Proposed harmonic compensation strategy.

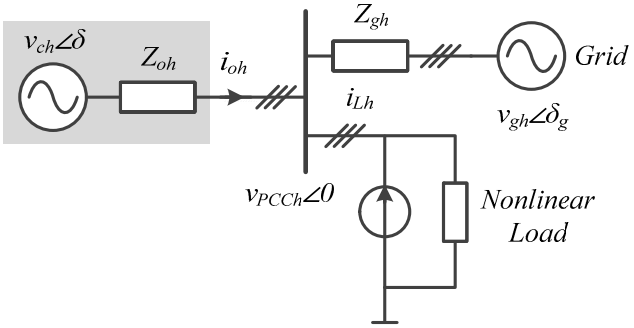

Fig. 4. Equivalent circuit of a converter connected to the grid.

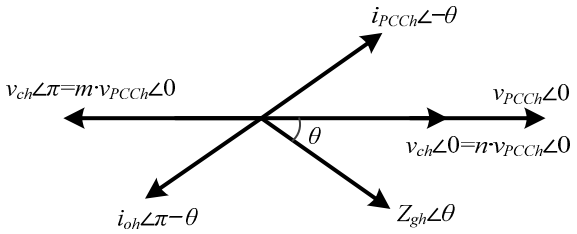

Fig. 5. Phasor diagram of a DG converter connected to the grid.

$$i_{oh} = \frac{K \cdot v_{PCCh}\angle 0 - v_{PCCh}\angle 0}{Z_{oh}} = v_{PCCh}\angle 0 \cdot \frac{K-1}{Z_{oh}} \tag{1}$$

From (1), operation modes of the HC can be concluded as: 1) harmonic compensation mode, if $K < 0$ ($m < 0$); 2) harmonic rejection mode, if $0 < K \le 1$ ($0 < n \le 1$). Note that $K > 1$ is not preferred, since it may induce harmonics into the system.

To ensure efficient and accurate harmonic voltage extraction, the Sliding Window Discrete Fourier Transform (SDFT) [7] is utilized in this paper. The corresponding calculation algorithm is given as

$$X_h = \sum_{n=0}^{N-1} x(n) \cdot \cos\left(\frac{2\pi hn}{N}\right) - j\sum_{n=0}^{N-1} x(n) \cdot \sin\left(\frac{2\pi hn}{N}\right) \tag{2}$$

where X_h denotes the complex Fourier vector of the h^{th} harmonic, N denotes the number of samples per fundamental period, $x(n)$ denotes the input signal at the n^{th} sample point. From (2), the amplitude and phase angle of the h^{th} harmonic can be calculated after one fundamental cycle. And then, the harmonic voltage reference can be obtained after scaled by K.

IV. Design and Stability Analysis of the Proposed HC

A. Fundamental Current Control loop

The basic function of DG converter is regulating the power generation from the RES, and providing a unity power factor current to the grid. Generally, the converter output current I_o is controlled by a PR controller with a high gain at fundamental frequency. Thus, both positive and negative sequence output current can track its reference accurately. It is worth noting that 5th, 7th, or higher order resonant controllers are not involved, otherwise the current loop controller will be coupled with HC, and then instability issues may occur. Note that the DC voltage loop is not discussed in this paper, since it is usually designed with low bandwidth, and will not interact with the inner current loop. The current loop transfer function can be expressed as

$$G(s) = k_{ip} + k_{ir}\frac{s}{s^2 + \omega^2} \tag{3}$$

where k_{ip} and k_{ir} are the proportional coefficients and resonant coefficients of the current controller, respectively, ω is the fundamental angular frequency.

LCL filter can be approximate as a single L filter at fundamental frequency, since the filter capacitor presents as high impedance for low frequency components. τ is tuned to cancel out the pole of the filter while k_{pi} is set to achieve the desired control bandwidth [8]. Note that this bandwidth should be smaller than 0.3 times of the *LCL* filter resonant frequency to avoid instability issues [9]-[10]. The controller parameters can be calculated as follows

$$k_{pi} = 2\pi f_c(L + L_g) \tag{4}$$

$$\tau = (L + L_g)/(r + r_g) \tag{5}$$

where f_c is the desired crossover frequency, L and L_g are the

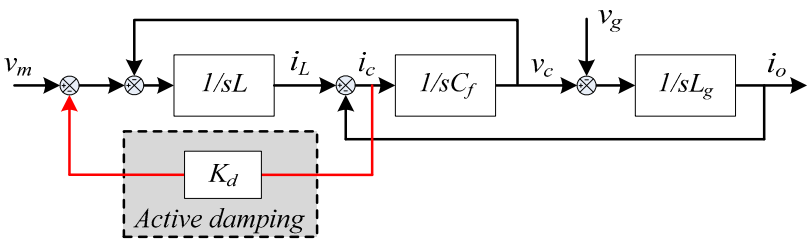

Fig. 6. Damped plant model.

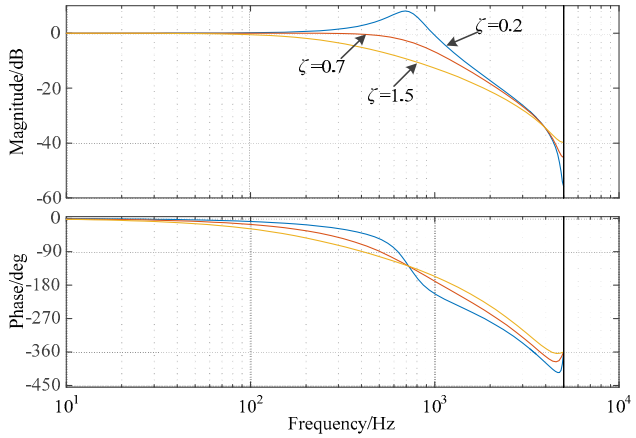

Fig. 7. Bode plot of the damped system.

converter side and grid side inductor, respectively, r and r_g are the parasite resistance of the converter side and grid side filter inductor, respectively. By using the system parameters listed in Table I, together with f_c =250Hz, the corresponding control parameters are eventually determined as k_{pi} =5.6, and τ =0.009.

B. Active Damping

Since the resonant frequency of *LCL* filter in this case lies out of the inherent stable range, i.e. the filter resonant frequency is lower than one sixth of the system sampling frequency [11]-[12], an extra active damping term is needed to stabilize the system. In this paper, capacitor current feedback based active damping is utilized [12]. By neglecting parasitic parameters of the *LCL* filter, the damped power plant model is shown in Fig. 7, and then the transfer function from converter output voltage v_m to grid current i_o in s-domain is derived in (6) and (7).

$$G(s)=\frac{i_o}{v_m}=\frac{1}{s\left(LL_gC_fs^2+K_dL_gC_fs+(L+L_g)\right)}=\frac{1}{LL_gC_f}\cdot\frac{1}{s\left(s^2+2\xi\omega_{res}s+\omega_{res}^2\right)} \tag{6}$$

$$K_d=2\xi L_g\omega_{res}=2\xi L_g\sqrt{\frac{L+L_g}{LL_gC_f}} \tag{7}$$

where C_f is the filter capacitor, K_d is the capacitor current feedback gain, ξ is the damping ratio while ω_{res} is the *LCL* filter resonant frequency. From (6), it can be seen that by proper tuning of the feedback gain K_d, a second order system with desired damping ratio can be obtained.

TABLE I. SYSTEM PARAMETERS

Elements	*Parameters*	*Value*
Converter	Converter Side Inductors L	1.8 mH
	Grid Side Inductors L_g	1.8 mH
	Capacitors C_f	9 μF
	Parasite resistor in Inductors r	0.2 Ω
	Nominal Voltage V	230 V
	Nominal Frequency f	50 Hz
	DC Voltage V_{DC}	650 V
	Switching Frequency f_s	10 kHz
Nonlinear Load	Three phase diode rectifier	---
	DC smoothing inductor	100 μH
	DC load	70 Ω

Finally, K_d is determined as 9 with the desired damping ratio 0.4.

C. Harmonic Voltage Control Loop

Although the active damping is implemented in this paper to damp the power plant for fundamental current control loop, unfortunately extra phase lag is also introduced in the capacitor voltage feedback loop. The induced phase shift can be neglected at fundamental frequency, however, this issue becomes worse in high frequency applications, such as active filtering field. To clarify this issue, the power plant transfer function for harmonic compensation loop is derived as

$$G_p(s)=\frac{v_c}{v_m}=\frac{1}{LC_fs^2+K_dC_fs+1} \tag{8}$$

Since the controller is commonly implemented in a digital manner, the plant transfer function is thus discretized through Zero-Order Hold (ZOH) method before being used for stability analysis and the derivation is listed in the appendix. Bode plot of the discretized plant transfer function is depicted in Fig. 7 with different damping ratio ξ. It can be seen that the resonance peak is effectively damped thanks to the active damping loop. However, a noticeable phase lag appears in the loop gain at frequencies lower than the resonant frequency. Thus, it would be critical to compensate those phase lags to obtain a better compensation performance. In this paper, HC based on resonant controllers [13] is proposed to compensate the phase lag induced by active damping as well as computational delay and PWM process. Transfer function of the resonant controller can be expressed in the z-domain as

$$G_{resh}(z)=k_{res}T_s\frac{\cos\varphi_c-z^{-1}\cos\left(\varphi_c-h\omega T_s\right)}{1-2z^{-1}\cos\left(h\omega T_s\right)+z^{-2}} \tag{9}$$

where k_{res} is the gain of the resonant controller, h is the order of the harmonic, T_s is the sampling period, and φ_c is the leading

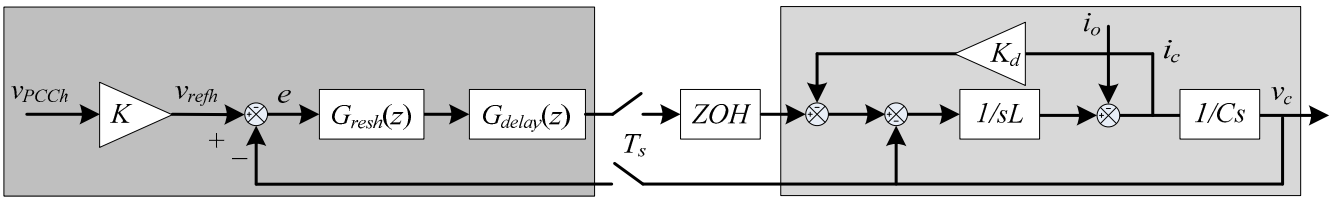

Fig. 8. Control block of the harmonic compensation loop.

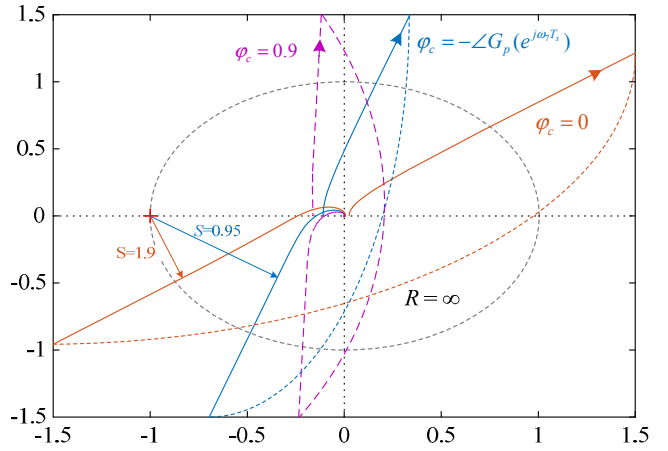

Fig. 9. Nyquist diagram of (12) with φ_{c7} equals to 0, 0.9, and $-\angle G_p(e^{j\omega_7 T_s})$. Parameters: $K_d = 9$, and $K_r = 100$.

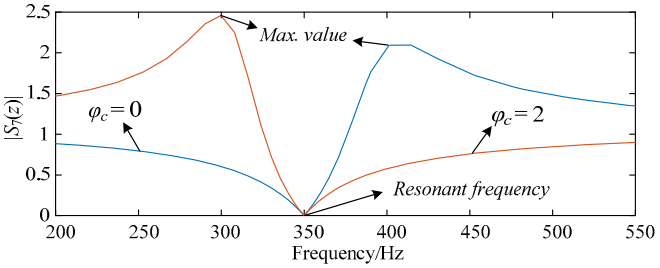

Fig. 10. Modulus of $S_7(z)$ with different compensation angle.

angle at the resonant frequency. The resonant controller is discretized by impulse invariant (IMP) method [14] since an acceptable compromise can be obtained between accuracy and computational burden. Also note that HC includes a set of $G_{resh}(z)$ to compensate multiple order harmonics.

By taking the time delay caused by calculation and PWM process into consideration, the damped power plant model along with the voltage HC control loop in z-domain is depicted in Fig. 8. Consequently, open loop transfer function of the harmonic compensation loop is derived as

$$G_{ol}(z) = G_{resh}(z)G_{delay}(z)G_p(z) \tag{10}$$

where $G_p(z)$ and $G_{delay}(z)$ denote the z-domain transfer function of the power plant and the computational delay, respectively. Note that the PWM delay is modeled by ZOH [15].

To assess the relationship between the current controller parameters and the system stability region, Nyquist stability criterion is utilized in this paper since it can not only tell whether the system is stable or not, but also give an accurate stability margin in terms of sensitivity function [16], [17]. Considering the system shown in (10), the system error is given by

$$E(z) = \frac{K \cdot v_{PCCh}(z)}{1 + G_{ol}(z)} = S(z) \cdot K \cdot v_{PCCh}(z) \tag{11}$$

where $S(z)$ is the defined sensitivity function. In addition to being a factor of the system error, the sensitivity function $S(z)$ is also the reciprocal of the distance from the Nyquist trajectory, $G_{ol}(z)$, to the critical point. The maximum value of the sensitivity function is known as the sensitivity peak which offers a more accurate measure of stability margin than either phase or gain margin would indicate.

By combining the designed control gains with the passive component parameters listed in Table I, the open loop transfer function of the 7th order harmonic compensation loop is derived as

$$G_{ol7}(z) = G_{res7}(z)G_p(z)G_{delay}(z)$$
$$= \frac{(0.0043z^4 + 0.0036z^3)(\cos\varphi_{c7} - \frac{\cos(\varphi_{c7} - h\omega T_s)}{z})}{z^6 - 3.399z^5 + 4.432z^4 - 2.631z^3 + 0.6065z^2} \tag{12}$$

where φ_{c7} is the leading angle of 7th order resonant controller.

Nyquist diagram of (12) is then illustrated in Fig. 9. The orange curve corresponding to the open loop system without delay compensation, while the blue curve stand for the system with φ_{c7} equals to the system phase lag at 7th order harmonic frequency. Fig. 9 shows that $S(z)$ of the compensated system (blue curve) is almost 2 times smaller than that of the uncompensated system (orange curve), which indicates the compensated system have a bigger stability margin. By further increasing φ_{c7}, the stability margin can be further improved and reach its maximum value when φ_{c7} equals to 0.9. However, since φ_{c7} will deviate from the real phase lag of the system, this improved stability margin is obtained at the expense of compensation accuracy degradation.

In order to dig out the influence of φ_{c7} to stability margin, sensitivity function of the system is derived as

$$S_7(z) = \frac{1}{D_7(z)} = \frac{1}{1 + G_{res7}(z)G_p(z)G_{delay}(z)} \tag{13}$$

where $D_7(z)$ denotes the vector from the Nyquist curve to the critical point. The modulus of $S_7(z)$, which is the reciprocal of the distance from Nyquist curve to the critical point, is shown in Fig. 10 with φ_{c7} equals to 0 and 2, respectively. As it can be seen, $S_7(z)$ varies along with the changing of φ_{c7}. $|S_7(z)| = 0$ means the Nyquist curve is at infinite which is caused by the infinite gain of $G_{res7}(z)$ at resonant frequency. Meanwhile, the

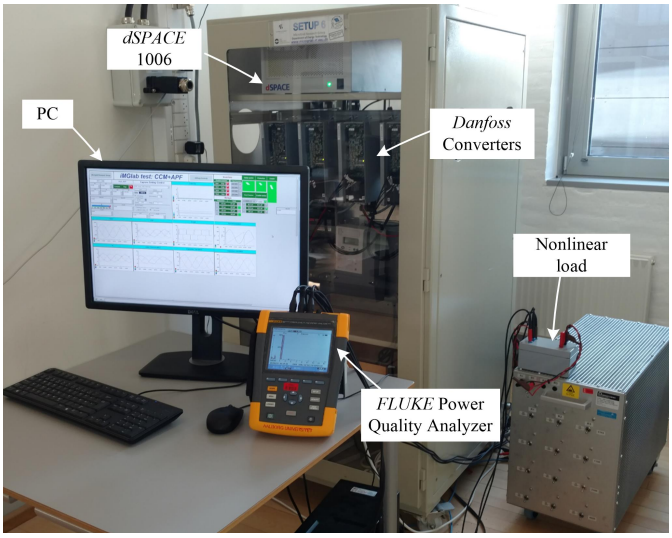

Fig. 11. Experimental platform.

TABLE II. RESONANT CONTROLLERS PARAMETERS

Parameters	Symbol	Value
Proportional Gain	k_{pi}	5.6
Time Constant	τ	0.009
Resonant Controllers Leading Angle	φ_{c5}	0.41
	φ_{c7}	0.61
	φ_{c11}	1.11
	φ_{c13}	1.38
Capacitor Current Feedback Gain	K_d	9

maximum value of $|S_7(z)|$ denotes minimum distance from the Nyquist curve to the critical point, and this value accurately indicates the stability margin of the system.

In general, the leading angle is set to be equal to the system delay at the resonant frequency to achieve large stability margin as well as high compensation accuracy. However, a higher stability margin can be achieved by further reducing the sensitivity function at the expense of lower the resonant controller tracking accuracy. Thus, by following the same design procedure, resonant controllers tuned at 5th, 11th, and 13th order harmonics are designed by minimizing the sensitivity function, and all the designed control parameters are listed in Table II.

V. EXPERIMENTAL RESULTS

In order to validate the proposed control strategy, experimental study is conducted and the results are included below. The experimental platform [18], which consists of two 2.2kVA converters in three-phase three-leg connection with *LCL* filters, is shown in Fig. 11. One of the converters is utilized to emulate DG converter while the other converter is programmed to emulate the grid. Three-phase diode rectifier with *L* filter and resistive load is connected to PCC to emulate the nonlinear load. Specifications of power stage and control system are given in Tables I and II. A real time control system is utilized to control the experimental platform while *FLUKE* 437-II power quality analyzer is employed to monitor the harmonic conditions.

Figs. 12 and 13 show the PCC voltage and its spectrum

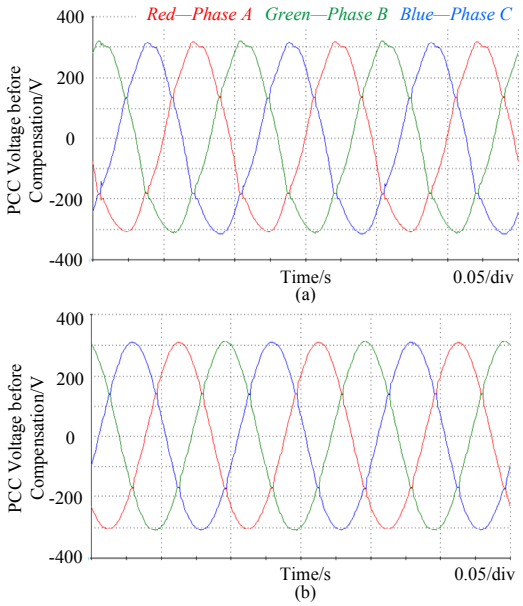

Fig. 12. PCC voltage. (a)before compensation. (b)after compensation.

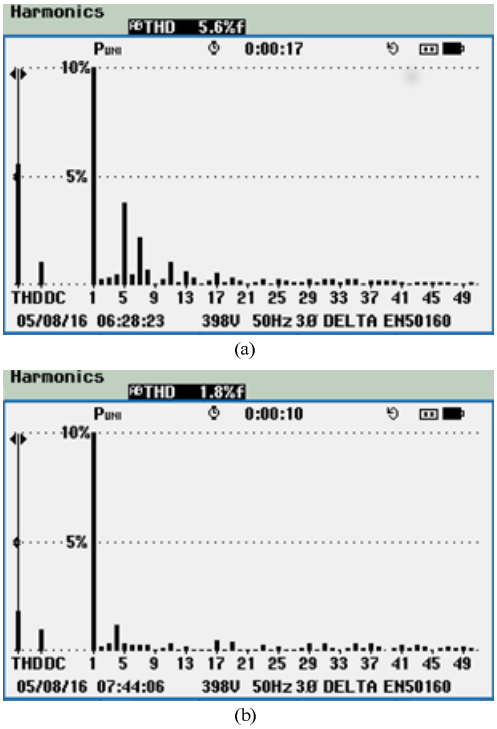

Fig. 13. PCC voltage spectrum and THD. (a)before compensation. (b)after compensation.

before and after the harmonic compensation, respectively. As it can be seen, PCC voltage becomes more sinusoidal after the proposed compensation strategy is activated and the corresponding total harmonic distortion (THD) drops significantly from 5.6% to 1.8%. Moreover, Fig. 13 illustrates that all the compensated harmonics (5th, 7th, 11th, and 13th order) drops dramatically. To clearly reveal the harmonic voltage mitigation performance, transient response of the PCC voltage harmonic distortion (defined by the quotient of harmonic amplitude divided by amplitude of fundamental

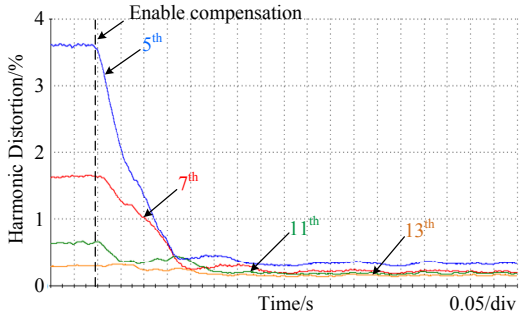

Fig. 14. 5th, 7th, 11th, and 13th order voltage harmonic distortion.

component) is depicted in Fig. 14. It is observed that with the proposed controller, 5th, 7th, 11th, and 13th order voltage harmonic distortion have been significantly reduced, as expected in controller design part.

VI. Conclusion

In this paper, a novel voltage harmonic compensation strategy based on harmonic voltage control has been investigated. The control structure includes three parts: the fundamental current loop, harmonic voltage loop and active damping controller. The proposed voltage harmonic control loop can seamlessly integrate with the fundamental current control loop. Compared with the conventional harmonic compensation strategy, the proposed scheme has the advantage of no remote current measurement and high compensation accuracy. Moreover, it offers the possibility of compensation efforts sharing with other CCM or VCM operated units which is a desirable feature under the paradigm of distributed generation. The effectiveness of the control scheme has been validated with one converter connected to the grid through *LCL* filter. The experimental results show that the PCC voltage harmonics decreased significantly after the harmonic voltage control loop is enabled.

References

[1] H. Akagi, H. Fujita, and K. Wada, "A shunt active filter based on voltage detection for harmonic termination of a radial power distribution line," *IEEE Trans. Ind. Appl*., vol. 35, no. 3, pp. 638–645, Jun 1999.

[2] R. Bojoi, L. R. Limongi, D. Roiu, A. Tenconi, "Enhanced Power Quality Control Strategy for Single-Phase Inverters in Distributed Generation Systems," *IEEE Trans Power Electron*., vol. 26, no. 3, pp. 798–806, Mar. 2011.

[3] X. Sun, R. Han, H. Shen, B. Wang, Z. Lu, and Z. Chen, "A Double-Resistive Active Power Filter System to Attenuate Harmonic Voltages of a Radial Power Distribution Feeder," *IEEE Trans. Power Electron*., vol. 31, no. 9, pp. 6203–6216, Sept. 2016.

[4] M. Savaghebi, A. Jalilian, J. C. Vasquez, J. M. Guerrero, "Secondary Control for Voltage Quality Enhancement in Microgrids," *IEEE Trans. Smart Grid*, vol. 3, no. 4, pp. 1893–1902, Dec. 2012.

[5] J. He, Y. Li, M. S. Munir, "A Flexible Harmonic Control Approach Through Voltage-Controlled DG–Grid Interfacing Converters," *IEEE Trans. Ind. Electron*., vol. 59, no. 1, pp.444–455, Jan. 2012.

[6] Y. Li, J. He, "Distribution System Harmonic Compensation Methods: An Overview of DG-Interfacing Inverters," *IEEE Trans. Ind. Electron*., Mag., vol. 8, no. 4, pp. 18–31, Dec. 2014.

[7] E. Jacobsen, R. Lyons, "The sliding DFT," *IEEE Signal Processing Mag*., vol. 20, no. 2, pp. 74–80, Mar. 2003.

[8] L. Harnefors, A. G. Yepes, A. Vidal, and J. Doval-Gandoy, "Passivity-Based Controller Design of Grid-Connected VSCs for Prevention of Electrical Resonance Instability," *IEEE Trans. Ind. Electron*., vol. 62, no. 2, pp. 702–710, Feb. 2015.

[9] L. Harnefors, X. Wang, A. G. Yepes, and F. Blaabjerg, "Passivity-Based Stability Assessment of Grid-Connected VSCs," *IEEE Journal of Emerging and Selected Topics in Power Electron*., vol. 4, no. 1, pp. 116–125, March 2016.

[10] Y. Tang, P. C. Loh, P. Wang, F. H. Choo, and F. Gao, "Exploring inherent damping characteristic of LCL-filters for three-phase grid-connected voltage source inverters," *IEEE Trans. Power Electron*., vol. 27, no. 3, pp. 1433–1443, Mar. 2012.

[11] S. G. Parker, B. P. McGrath, and D. G. Holmes, "Regions of Active Damping Control for LCL Filters," *IEEE Trans. Ind. Appl*., vol. 50, no. 1, pp. 424–432, Jan.–Feb. 2014.

[12] D. Pan, X. Ruan, C. Bao, W. Li, and X. Wang, "Capacitor-Current-Feedback Active Damping With Reduced Computation Delay for Improving Robustness of LCL-Type Grid-Connected Inverter," *IEEE Trans. Power Electron*., vol. 29, no. 7, pp. 3414–3427, Jul. 2014.

[13] R. I. Bojoi, G. Griva, V. Bostan, M. Guerriero, F. Farina, and F. Profumo, "Current control strategy for power conditioners using sinusoidal signal integrators in synchronous reference frame," *IEEE Trans. Power Electron*., vol. 20, no. 6, pp. 1402–1412, Nov. 2005.

[14] A. G. Yepes, F. D. Freijedo, J. Doval-Gandoy, O. López, J. Malvar, and P. Fernandez-Comesaña, "Effects of Discretization Methods on the Performance of Resonant Controllers," *IEEE Trans. Power Electron*., vol. 25, no. 7, pp. 1692–1712, July 2010.

[15] S. Buso and P. Mattavelli, *Digital Control in Power Electronics.* San Francisco, CA, USA: Morgan & Claypool, 2006.

[16] G. F. Franklin, J. D. Powell, and M. Workman, *Digital Control of Dynamic Systems*, NJ, USA: Ellis-Kagle Press, 2000.

[17] A. G. Yepes, F. D. Freijedo, O Lopez, and J. Doval-Gandoy, "Analysis and Design of Resonant Current Controllers for Voltage-Source Converters by Means of Nyquist Diagrams and Sensitivity Function," *IEEE Trans. Ind. Electron*., vol. 58, no. 11, pp. 5231–5250, Nov. 2011.

[18] www.microgrids.et.aau.dk

Appendix

$$
\begin{aligned}
G_p(z) &= Z\left\{\frac{1-e^{-sT}}{s}\cdot G_p(s)\right\} \\
&= \left(1-z^{-1}\right)\cdot Z\left\{\frac{G_p(s)}{s}\right\} \\
&= \left(1-z^{-1}\right)\cdot Z\left\{\frac{1}{s\left(LCs^2+K_dCs+1\right)}\right\} \\
&= \left(1-z^{-1}\right)\cdot Z\left\{\frac{\frac{1}{LC}}{s\left(s^2+\frac{K_d}{L}s+\frac{1}{LC}\right)}\right\} \\
&= \left(1-z^{-1}\right)\cdot Z\left\{\frac{\omega_0^2}{s\left(s^2+2\xi_0\omega_0 s+\omega_0^2\right)}\right\} \\
&= \left(1-z^{-1}\right)\cdot \\
&\quad \left\{\frac{z}{z-1}-\frac{1}{\sqrt{1-\xi_0^2}}\cdot\frac{z^2\sqrt{1-\xi_0^2}+ze^{-\xi_0\omega_0T}\sin\left(\omega_0\sqrt{1-\xi_0^2}T-\varphi\right)}{z^2-2ze^{-\xi_0\omega_0T}\cos\left(\omega_0\sqrt{1-\xi_0^2}T\right)+e^{-2\xi_0\omega_0T}}\right\} \\
&= 1-\frac{z-1}{\sqrt{1-\xi_0^2}}\cdot\frac{z\sqrt{1-\xi_0^2}+e^{-\xi_0\omega_0T}\sin\left(\omega_0\sqrt{1-\xi_0^2}T-\varphi\right)}{z^2-2ze^{-\xi_0\omega_0T}\cos\left(\omega_0\sqrt{1-\xi_0^2}T\right)+e^{-2\xi_0\omega_0T}}
\end{aligned}
$$

where $\omega_0 = 1/\sqrt{LC}$, $\xi_0 = 0.5K_d\sqrt{C/L}$, and $\varphi = \arccos\xi_0$.